





PAPER

Electrothermal shape memory behavior and recovery force of four-dimensional printed continuous carbon fiber/polylactic acid composite

To cite this article: Haijia Chen *et al* 2021 *Smart Mater. Struct.* **30** 025040

View the [article online](#) for updates and enhancements.

Electrothermal shape memory behavior and recovery force of four-dimensional printed continuous carbon fiber/polylactic acid composite

Haijia Chen¹, Fenghua Zhang², Ya Sun¹, Baozhong Sun¹ , Bohong Gu¹ , Jinsong Leng²  and Wei Zhang¹ 

¹ Shanghai Collaborative Innovation Center for High Performance fiber composites, College of Textiles, Donghua University, Shanghai 201620, People's Republic of China

² Center for Composite Materials and Structures, Harbin Institute of Technology, Harbin 150080, People's Republic of China

E-mail: weizhang@dhu.edu.cn and lengjs@hit.edu.cn

Received 4 October 2020, revised 7 December 2020

Accepted for publication 6 January 2021

Published 25 January 2021



Abstract

Four-dimensional (4D) printing technology provides new ideas for the preparation and structural design of multifunctional shape memory composites. Excellent electrothermal shape memory behavior and high shape recovery force are urgently demanded in practical applications. Herein, a continuous carbon fiber reinforced polylactic acid shape memory composite with high strength, high shape recovery force, low-voltage response and excellent electrothermal shape memory behavior was printed using a dual nozzle 3D printer. The effects of specimen thickness, carbon fiber content, and applied voltage on the electrothermal shape memory behavior and shape recovery force were investigated. The reinforcing effect of carbon fiber on 4D printed composite materials was characterized by dynamic mechanical analysis and 3-point bending test. Under electrical thermal stimulation, the shape recovery ratio of most specimens can reach 90%. The shape recovery force of different specimens was obtained by self-designed shape recovery force test system, and the maximum shape recovery force was about 7.38 N. The results show that the introduction of continuous carbon fiber not only significantly enhances the strength of 4D printed composite, but also improves the shape recovery force. The demonstrations of an electrothermal response shape memory deployable claw-device and load-bearing lifting device manifest the potential application in self-actuated intelligent structures.

Supplementary material for this article is available [online](#)

Keywords: 4D printing, continuous carbon fiber, shape memory composite, electrothermal activation, shape recovery force

(Some figures may appear in colour only in the online journal)

1. Introduction

Four-dimensional (4D) printing is the extension of the time dimension based on 3D printing and a combination of smart materials and structural design, bringing revolutionary

innovation to materials and self-assembly equipment [1, 2]. Stimulus-response materials are a type of smart materials, which can evolve with time when it is exposed to an external stimulus, such as light [3, 4], electricity [5, 6], temperature [7–11], solution [12, 13], pH [14, 15], magnetic field [16, 17]

and microwave [18], etc. As one of the most widely used 4D printing materials, shape memory polymers (SMPs) have initiated various researches and applications in the fields of tissue-engineering [19, 20] and soft robots [21–23] owing to the advantages of a lightweight, large deformation, easy processing, etc. However, pure SMPs exhibit low modulus and can only activate the shape memory process under thermal stimulation. To overcome these limitations, some researchers have developed conductive composites by combining SMPs with conductive fillers, including particles [24–27], fibers [28–31] or polypyrrole [32]. For instance, Liu *et al* [26] investigated the electrothermal properties and electro-activated shape memory behavior at high DC voltages (>120 V) of carbon nanotube (CNT)/polylactic acid (PLA) composite. Garces *et al* [27] used shape memory polyurethane and graphene PLA to prepare electrically activated composites by additive manufacturing. The influences of strain and electrothermal temperature on the resistance of composites were studied, and the results showed that strain and temperature have a significant influence on the resistance. Zeng *et al* [31] studied the bending resistance of 4D printed continuous carbon fiber reinforced SMP composites, and concluded that the composite has excellent bending resistance and electro-induced shape memory effect.

Shape recovery force is an important indicator used to characterize shape recovery ability. Some researchers have conducted some research on it. Gall *et al* [33] studied the effect of SiC filler on shape recovery force under displacement constraint in the DMA, it is concluded that SMP can only generate 300 mN, while 20% wt SiC reinforced SMP can generate 450 mN. Chen *et al* [34] investigated the influence of width on the recovery force of pure ESMP specimens by a DMA instrument under fixed displacement, and the shape recovery force of the specimen with a width of 12 mm was 450 mN. Liu *et al* [35] studied the effect of carbon nanotube filler and silicone elastomer matrix on shape recovery force of 4D printed composites in DMA 3-point bending mode, the maximum recovery force of CNT/PLA angle-ply laminated preform/silicone matrix composite is 1.28 N among all composite materials. Monzón *et al* [36] developed a test bench to measure the recovery force of the 3D printed SMP. Song *et al* [37] used a custom-built electronic force sensor with a cantilever design to measure the recovery force of pre-strained TPU/PLA blends and pure TPU samples under free strain conditions, and the results showed that 80/20 TPU/PLA blends have excellent shape recovery performance and maximum shape recovery force. But there is currently no standard test equipment for the shape recovery force test of polymers and their composites, also there are relatively little researches on the shape recovery force. Besides, there are still some problems in the current literature, such as the poor conductivity of the prepared specimen, the high activation voltage and low strength.

Therefore, this paper focus on the improvement of electrothermal activation response properties, strength and shape recovery force of 4D printed structures. We prepared a 4D printed continuous carbon fiber reinforced PLA (CCF/PLA) composite with a new dual-nozzle 3D printer. The shape memory PLA was used as the matrix and the CCF composite filament was used as the reinforcement material. This printed

Table 1. Printing parameters.

Printing parameters	materials	
	PLA	CCF
Diameter (mm)	1.75	0.4
Nozzle diameter (mm)	0.8	0.5
Layer height (mm)	0.125	0.125
Printing temperature (°C)	260	260
Print route	±45° (figure 1(b))	A-type and B-type

composite could respond stimulated by *in situ* electrical heating using the electric carbon fiber component. The 3-point bending and thermomechanical properties of 4D printing composites were characterized. The effects of specimen thickness, layers of carbon fiber and applied voltage on shape memory electrothermal behaviors were studied. Also, we developed a self-assembly design recovery force test system to measure the electrothermal shape recovery force. Finally, we demonstrated potential applications of a deployable claw-device and a load-bearing lifting device used in the self-actuated intelligent structural field.

2. Experimental section

2.1. Material and specimen fabrication

The PLA-based SMP filament with a diameter of 1.75 mm was provided by the Harbin Institute of Technology (HIT). PLA filament was dried in a vacuum drying oven for 24 h before printing. The continuous carbon fiber composite filament impregnated with nylon (abbreviated as CCF) with a diameter of 0.4 mm is a raw material specially used for Markforged X7 dual nozzle 3D printer. The CCF and printer were purchased from Markforged Co., Ltd The processing temperature of this CCF filament was 260 °C, and the volume fraction of carbon fiber in the CCF filament was 55.3%.

All specimens were printed by Markforged X7 3D printer with two printing nozzles for the deposition of pure PLA and CCF, respectively. 4D printing composite preparation process was shown in figure 1(a). Firstly, a printing model was established by CATIA software, and then the model was imported into Eiger software to complete the printing parameter settings (parameter in table 1). In addition, all CCF were deposited in the middle of the specimen, the bottom and top layers of the specimen were printed with 100% solid fill PLA matrix, and the PLA printing route was shown in figure 1(b). Figures 1(c) and (d) show the carbon fiber printing routes designed in two ways, A-type and B-type, and the corresponding specimens were printed. Different types of printed specimens were used according to different test items, which will be explained below.

2.2. Characterizations

The cross-section morphology of the CCF filament and CCF/PLA was observed using a scanning electron microscope (SEM) (JCM-6000PLUS, JEOL. Ltd Japan) with an

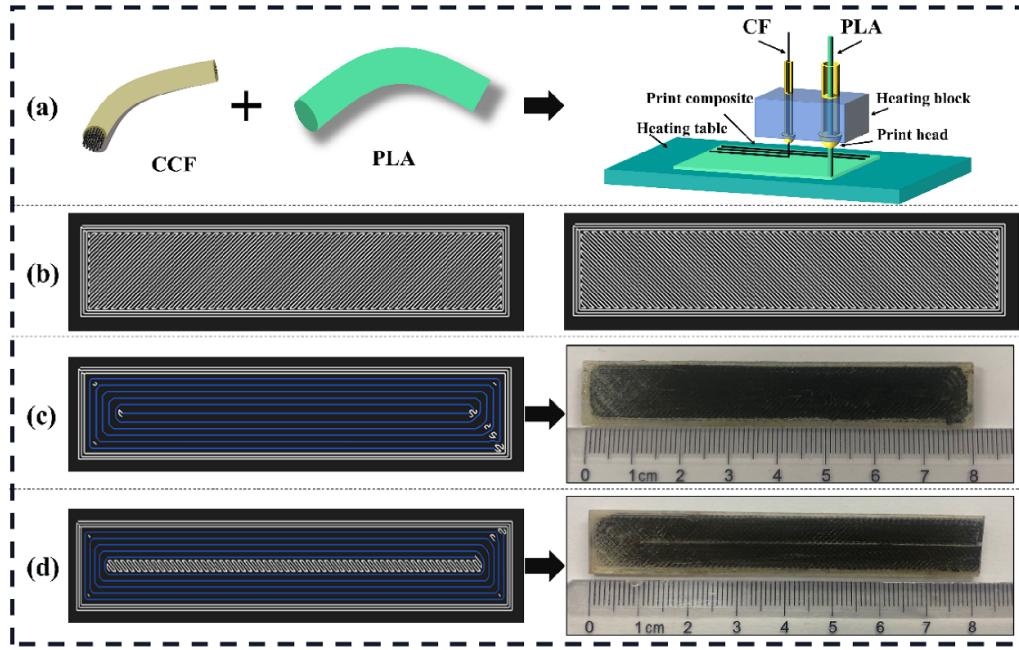


Figure 1. (a) The printing process of the 4D printed CCF/PLA composite. (b) Printing route of PLA. (c) The left is the A-type carbon fiber printing route, and the right is the printed specimen. (d) The left is the B-type carbon fiber printing route, and the right is the printed specimen.

accelerating voltage of 15.0 kV. To understand the glass transition temperature and melting temperature of PLA filaments, the thermal properties of PLA filaments were measured by differential scanning calorimetry (DSC, 204 F1) from 30 °C to 200 °C at a heating rate of 5 °C min⁻¹ in a nitrogen atmosphere. The specimen weight was around 5 mg and three specimens were tested.

2.3. Dynamic mechanical analysis and 3-point bending test

The DMA of 4D printed PLA and CCF/PLA specimens were conducted using the TA instrument DMA (Q800) with a temperature ramp from 25 °C to 100 °C at the ramp rate of 5 °C min⁻¹. The clamp of DMA was 3-point bending, the test mode was multi-frequency-strain, the sweep mode was temperature sweep and the frequency was fixed at 1 Hz. Three specimens of each type were tested.

Three-point bending mechanical properties of 4D printed PLA and CCF/PLA specimen were carried out on a mechanical universal material testing machine (Instron 5967) under room temperature. Following the ASTM D7264 standard [38], the bending span is 40 mm, the loading rate of 2 mm min⁻¹ and three specimens of each type were loaded until failure. The specimen type used for the DMA test and 3-point bending mechanical test was A-type, and the size of these specimens was 60 mm × 13 mm × 2 mm.

2.4. Electrothermal shape memory behavior characterization

The electrothermal shape memory behaviors of 4D printed CCF/PLA composite were characterized by the electrothermal properties of carbon fiber. The carbon fiber layers were

designed as B-type as shown in figure 1(d), and the length × width of the specimen were 80 mm × 13 mm. The purpose of this design was to guarantee the conductive connectivity of the carbon fiber inside the composite materials when a voltage was applied to one end of the specimen. The recording method of the electrothermal shape recovery behavior test process is shown in figure 2(a). A Nikon D750 video camera was used to record the shape recovery process of composite specimens, and an FLIR E8 infrared thermography was used to monitor the distribution and change of specimen surface temperature during the shape recovery process. Image processing software, ImageJ, was used to measure the recovery angles at different time points.

The test schematic of the shape recovery is shown in figure 2(b). Firstly, the original specimen (position 1) was heated and deformed 180° (position 2) using a tool with a curvature radius of 17 mm under an external load. Secondly, the external force was removed after completely cooled, and the bent specimen recovered a certain angle (θ_1) due to elastic recovery to obtain the fixed shape (position 3). Finally, the fixed specimen gradually returned to its original shape when applied voltages by a DC power. The shape recovery ratio R_r , which was used to characterize the shape memory performance, and was calculated using the equation:

$$R_r = \frac{\theta_2 - \theta_1}{180^\circ - \theta_1} \times 100\%. \quad (1)$$

The shape fixed ratio, R_f , was calculated using the equation:

$$R_f = \frac{180^\circ - \theta_1}{180^\circ} \times 100\% \quad (2)$$

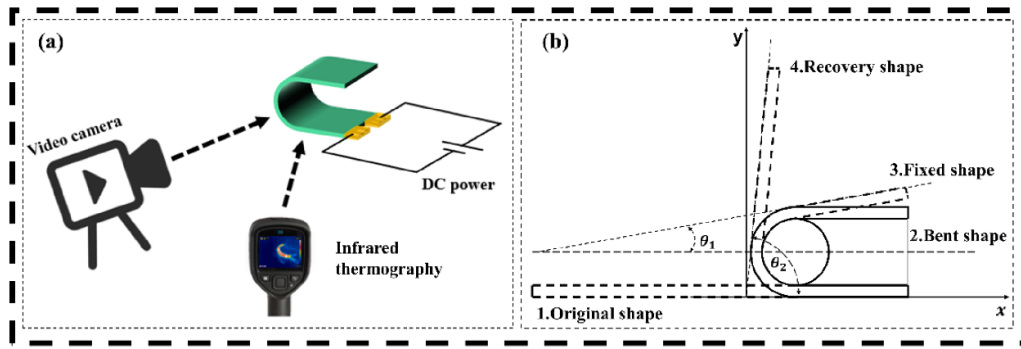


Figure 2. (a) The recording method of the electrothermal shape recovery behavior test process. (b) The test schematic of shape fixation and recovery.

where: $180^\circ - \theta_1$ was the shape fixed angle, and $\theta_2 - \theta_1$ was the shape recover angle. To understand the effect of applied voltage on the resistance of composite and choose suitable voltage for the test, we took the CCF/PLA 2L specimen as an example to test the relationship between current and applied voltage, as well as the relationship between temperature and applied voltage. A constant voltage was applied to both ends of the specimen. For each test, three specimens were tested.

2.5. Electrothermal shape recovery force test

In order to accurately measure the shape recovery force, a shape recovery force test system was designed and assembled by ourselves. The shape recovery force test system consists of two parts as shown in figure 3(a). One is the force acquisition system includes a force sensor (model: R105A-100 N, range: 0–100 N), an amplifier, a self-designed clamping device, and acquisition software. The self-designed clamping device is similar to a 3-point bending device with three fulcrums as shown in figure 3(b3). The pre-deformed specimen is clamped in the device and its displacement is limited by the fulcrum. The upper fulcrum connects the force sensor, which is used to obtain the force value changes when specimens try to recover their original shape once stimulated by the electrothermal. The other is the temperature acquisition system including a demodulator and K-type thermocouple. One end of the K-type thermocouple is connected to the demodulator and the other is fixed on the lower surface near the center of specimen to obtain real-time temperature changes of the specimen. Thus, the shape recovery force vs. temperature curves were obtained easily by the test system. This system records a temperature data point every 50 ms.

The process for the shape recovery force test includes three steps. Firstly, the original specimen (figure 3(b1)) was deformed into a ‘bow’ (figure 3(b2)) with a curvature radius of 42.5 mm, and then cooled to room temperature under constraint. Secondly, the ‘bow’ specimen was fixed to a 3-point bending fixture, and the sensor probe was adjusted to contact the specimen and fixed the sensor to limit its displacement as shown in figure 3(b3). At the same time fix the thermocouple to the specimen. Finally, the specimen recovers when applied voltages, and the specimen generates a force on the sensor. This force is recorded by the sensor, and the temperature of the specimen is recorded by the thermocouple. The length and

width of the A-type specimen used were 80 mm and 13 mm, respectively, and three specimens of each type were tested.

3. Results and discussion

3.1. Thermal properties and morphological characteristics

DSC measurement was conducted to characterize the thermal properties of the PLA filament, as shown in figure 4(a). The results show that the glass transition temperature (T_g) of the filament was around 60°C , the crystallization temperature and melting temperature were around 101°C and 175°C , respectively. In the subsequent characterization of shape memory performance, the pre-deformation temperature (T_d) was selected to be 100°C .

Figure 4(b) shows an SEM photograph of the CCF composite filament. It can be seen that carbon fibers were uniformly distributed in the CCF composite filament. The cross-sectional morphology of the CCF/PLA composite was also examined by SEM to observe the morphology of carbon fibers in the matrix and the distribution of voids in the composites as shown in figure 4(c). It can be seen that carbon fiber bundles evenly distribute in the 4D printed CCF/PLA composite (red circles in figure 4(c)), and only some small voids appear at the interface between the carbon fibers and the matrix (black circles area in figure 4(c)). This result indicates that the interface between the carbon fiber bundle and PLA is well bonded.

3.2. Thermomechanical properties and bending properties

Figure 5 shows the thermomechanical and mechanical properties of printed PLA and composite specimen. Figure 5(a) shows that the storage modulus of PLA decreases sharply while the loss modulus increases sharply after 45°C , the DMA test curve is interrupted when the temperature reaches around 52°C owing to the softening of PLA. This phenomenon reveals that PLA has viscoelasticity and temperature sensitivity. Figure 5(b) shows the storage modulus of CCF/PLA 2L rapidly decreases in the glass transition zone from 45°C to 65°C , and the loss modulus curve of the CCF/PLA 2L has a peak around 53°C between 45°C and 65°C in the transition zone. The Tan (δ) value of CCF/PLA 2L reaches a peak at 55.7°C , which can be considered as the glass transition temperature in the DMA mode. Figure 5(c) shows a comparison

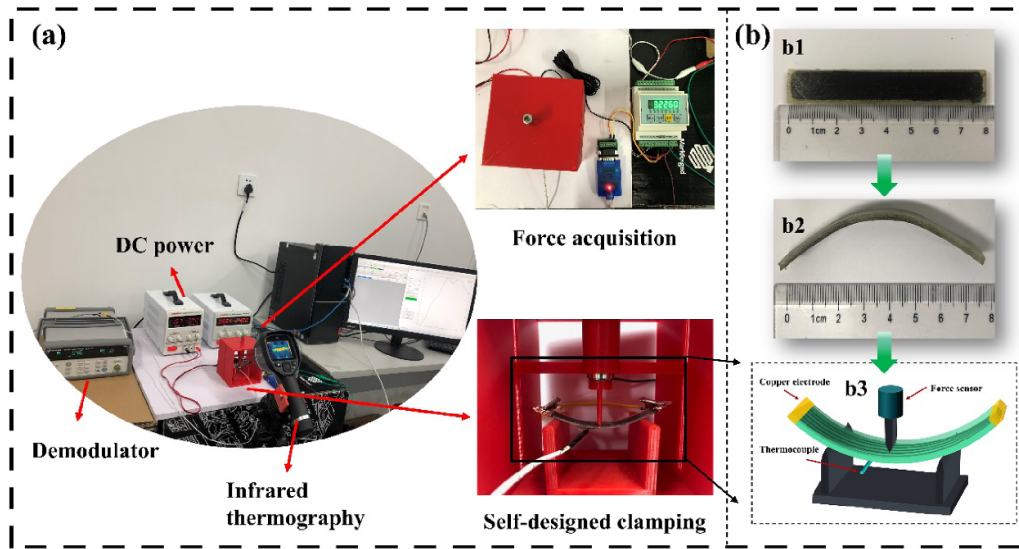


Figure 3. (a) The shape recovery force test system. (b) The schematic diagram of specimen assembly.

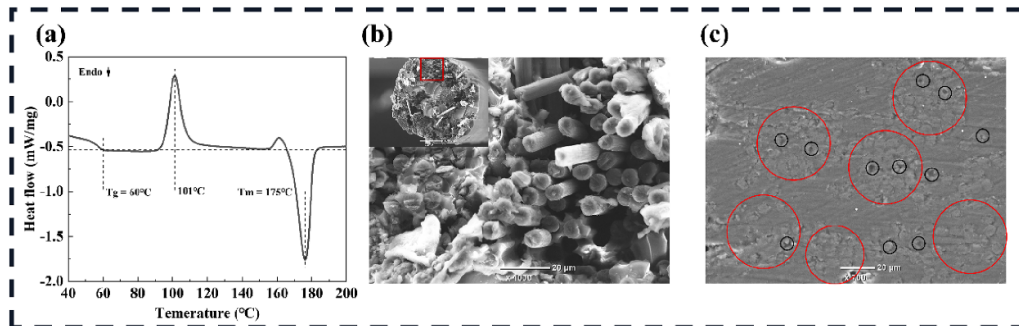


Figure 4. Characterizations. (a) The DSC curve of the PLA filament. (b) The SEM image of the CCF composite filament. (c) The cross-sectional SEM image of the CCF/PLA composite.

of the storage modulus of different specimen. It can be seen that the storage moduli of pure PLA, CCF/PLA 2L are almost the same, which is due to the low content of carbon fibers. The storage modulus of the specimen increases with the layers of carbon fiber. The storage modulus of CCF/PLA 6L reaches 5720 MPa, which is about twice that of pure PLA.

Figure 5(d) shows the 3-point bending load vs. displacement curve of specimen under room temperature. It can be seen that the failure displacement of PLA and CCF/PLA composites is <4.5 mm, and the maximum bending loads of PLA, CCF/PLA 2L, CCF/PLA 4L, and CCF/PLA 6L are 74.38 ± 2.5 N, 83.20 ± 1.7 N, 124.52 ± 3.6 N and 190.81 ± 4.2 N, respectively. The bending strength of the CCF/PLA composite increases with increasing the carbon fiber layers. Besides, the strength of CCF/PLA 6L is about 2.5 times that of pure PLA, which indicates that the introduction of CCF greatly enhances the mechanical properties of 4D printed CCF/PLA composite.

3.3. Electrothermal shape memory behavior

Figure 6(a) shows the voltage vs. current curve of CCF/PLA 2L specimen. It can be seen that the slope of the curve is almost

linear at lower voltage and increases slightly with increasing the voltage after 8 V, which shows that the resistance of the specimen increases slightly at higher voltage. This is attributed to the higher temperature generated by carbon fiber with higher resistance at applied higher voltage. Figure 6(b) shows the temperature vs. time curves of the CCF/PLA 2L specimen under three voltages. It can be seen that the temperature generated by the three voltages in a certain period can reach the T_g of the printed composite. The heating rate increases with increasing the voltage, and the electrothermal temperature increases with increasing the time. From the results, we can conclude that the applied three DC voltages were suitable for our experiment and the resistance effect of carbon fiber is little for our results.

The T1L2V7 means the CCF/PLA composite specimen with a thickness of 1 mm, two carbon fiber layers, and an applied voltage of 7 V. Figure 7(a) shows shape recovery ratio vs. time curves of 4D printed CCF/PLA composite with three different specimen thicknesses at the same carbon fiber layers of 2L under the applied voltage of 7 V. The shape recovery ratios of the specimens with thicknesses of 1 mm, 1.5 mm and 2 mm are around 98.2% in 115 s, 95.6% in 180 s and 87.1% in 240 s, respectively. From figure 7(d), we could get

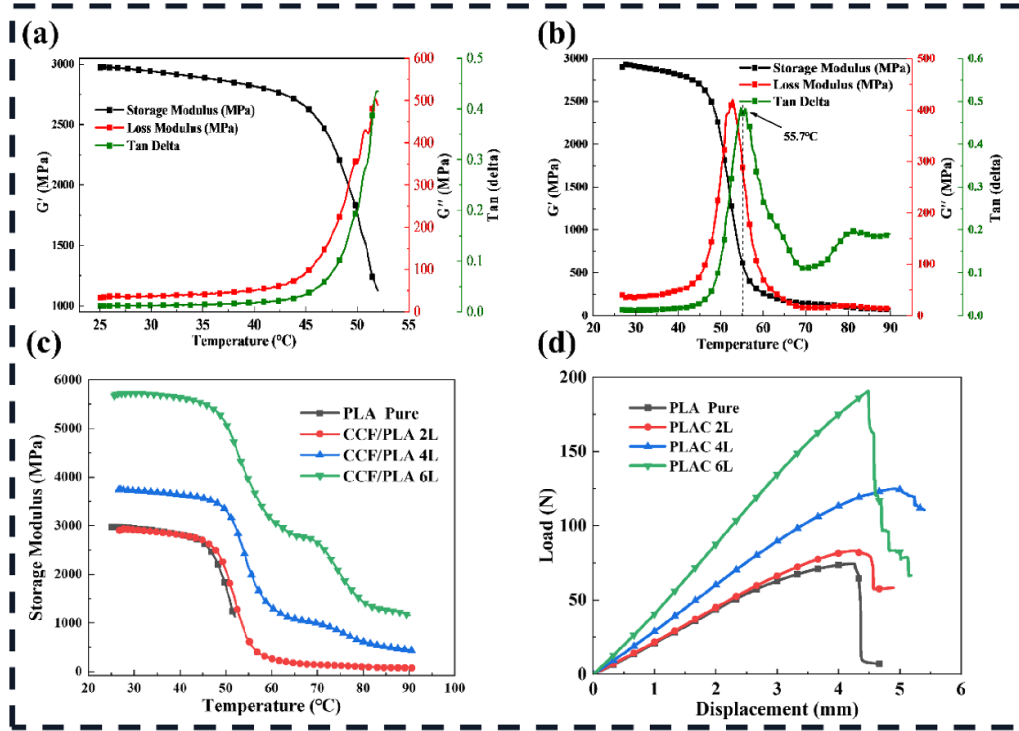


Figure 5. Thermomechanical and mechanical properties of specimens. The DMA results of (a) pure PLA, and (b) CCF/PLA 2L. (c) Comparison of storage modulus of PLA and CCF/PLA. (d) Three-point bending load vs. displacement curves of PLA and CCF/PLA composites.

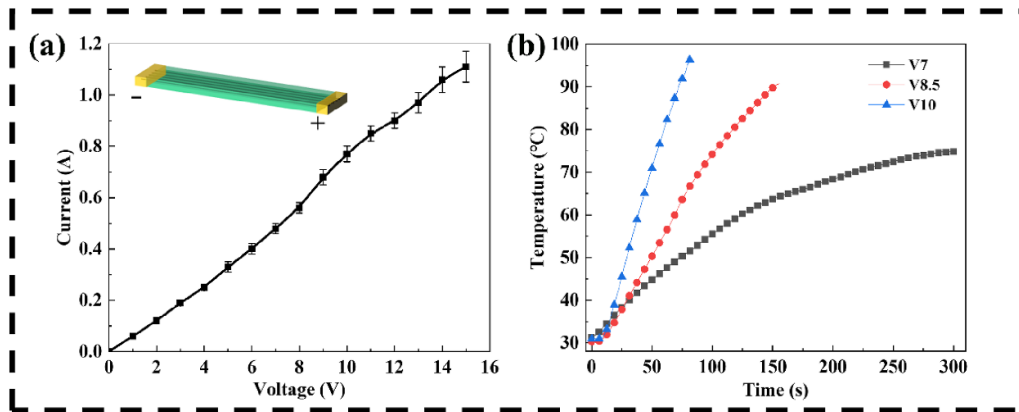


Figure 6. Electrical properties of CCF/PLA 2L specimen. (a) The curves of voltage and current. (b) The curves of temperature vs. time under different voltages.

the shape fixity ratios of the specimens with thicknesses of 1 mm, 1.5 mm and 2 mm are around 76.8%, 87.3%, and 90.0%, respectively. All the experimental error of the fixity ratio and final shape recovery ratio is <1.5%. From the above results, it can be seen that under the same carbon fiber layer and the same voltage, the shape recovery ratio decreases with increasing the thickness of the specimens, while the shape fixity ratio increases with increasing the thickness. The experimental results show that under the same carbon fiber layers, the specimen with a small thickness has a low reversible phase content in the PLA matrix, so the shape is difficult to fix and the shape fixity ratio is low, but the specimens with a small thickness have better elastic deformation recovery, thus, the high recovery ratio.

Figure 7(b) shows the shape recovery ratio vs. time curves of 4D printed CCF/PLA composite with three different applied voltages at same specimen thickness and same carbon fiber layers. The shape recovery time of the specimens at the three voltages of 7 V, 8.5 V, and 10 V is 240 s, 140 s, and 110 s, respectively. It can be seen that the shape recovery time decreases with increasing voltages, which is attributed to the high temperature generated under high voltage. The shape recovery ratios of the specimens at the three voltages of 7 V, 8.5 V, and 10 V are about 87.1%, 88.5%, and 93%, respectively. The shape fixity ratios of the specimens with different voltages are about 90%, 89.4%, and 89%, respectively as shown in figure 7(d). We can see that the shape fixity ratios at different voltages are almost the same, but the shape recovery

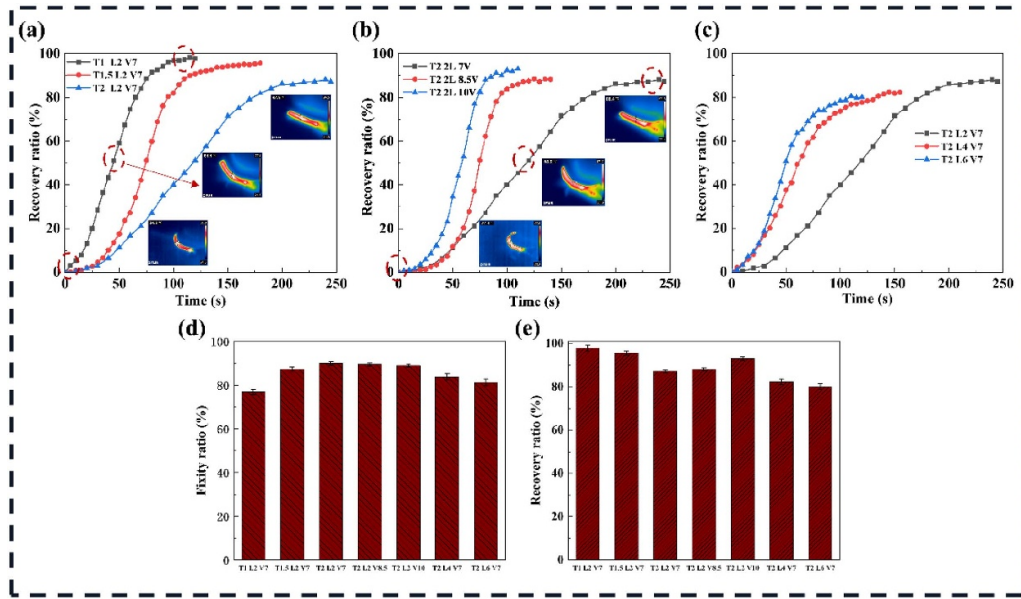


Figure 7. The shape recovery ratio vs. time curves of CCF/PLA (a) at three specimen thickness, (b) at three different voltages, and (c) at three different layers of carbon fiber. (d) The shape fixity ratio of different specimens. (e) The shape recovery ratio of different specimens.

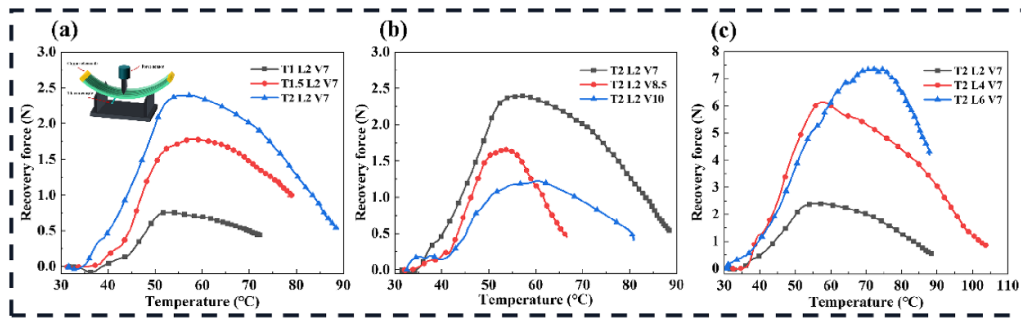


Figure 8. The shape recovery force vs. temperature curves of 4D printed CCF/PLA composites (a) at different specimen thicknesses, (b) at different voltages, and (c) at different carbon fiber layers.

ratios increase with increasing the voltage, which is due to the higher heat generated by the high voltage to promote the shape recovery.

Figure 7(c) shows the shape recovery ratio vs. time curves of CCF/PLA composite with three different carbon fiber layers at the same specimen thickness under the applied voltage of 7 V. The shape recovery ratios of the specimens with carbon fiber layers of 2L, 4L and 6L are around 87.1% in 240 s, 82.3% in 150 s, and 80.5% in 110 s, respectively. The shape fixity ratios of the specimens with three carbon fiber layers are around 89%, 83.8%, and 81.2%, respectively. We can know that the shape fixity ratio decreases with increasing the carbon fiber layer, which is due to the strength of the specimen with a large number of carbon fiber layers and the difficulty of bending deformation. Also, the shape recovery ratio decreases with increasing the carbon fiber layer. We analyzed two reasons for the decrease in the shape recovery ratio. The first is that as the number of carbon fiber layers increases, the PLA content relatively decreases, which reduces the shape recovery ratio. The second is due to the buckling failure [31] of the carbon fiber layer inside the specimen during the predetermined shape process, which caused the specimen to not fully

recover. All the curves are S-shaped, which shows that most of the shape recovery is completed in the middle period. The illustrations in figures 7(a) and (b) are infrared images of some specimens during the experiment, it can be seen that the temperature distribution on the surface of the specimen is uniform during the test. A detailed video of the electrothermal shape recovery process is shown in movie S1 (available online at stacks.iop.org/SMS/30/025040/mmedia).

3.4. Electrothermal shape recovery force

The shape recovery force was quantitatively and accurately measured by the self-designed and assembled shape recovery force test system. The change of the recovery force as a function of temperature can be divided into two stages as shown in figures 8(a)–(c). In the first stage, as the temperature increases from 30 °C to about 50 °C, the recovery force gradually increases and reaches a maximum at about 55 °C, which is between 50 °C and 60 °C in the temperature transition zone. In the second stage, the recovery force gradually decreases from the maximum with increasing the temperature. These results could be attributed to the fact that when the soft

Table 2. The maximum shape recovery force of different specimens.

Specimens	T1L2V7	T1.5L2V7	T2L2V7	T2L2V8.5	T2L2V10	T2L4V7	T2L6V7
Recovery force (N)	0.75 ± 0.01	1.78 ± 0.02	2.38 ± 0.03	1.65 ± 0.02	1.21 ± 0.02	6.12 ± 0.03	7.38 ± 0.03

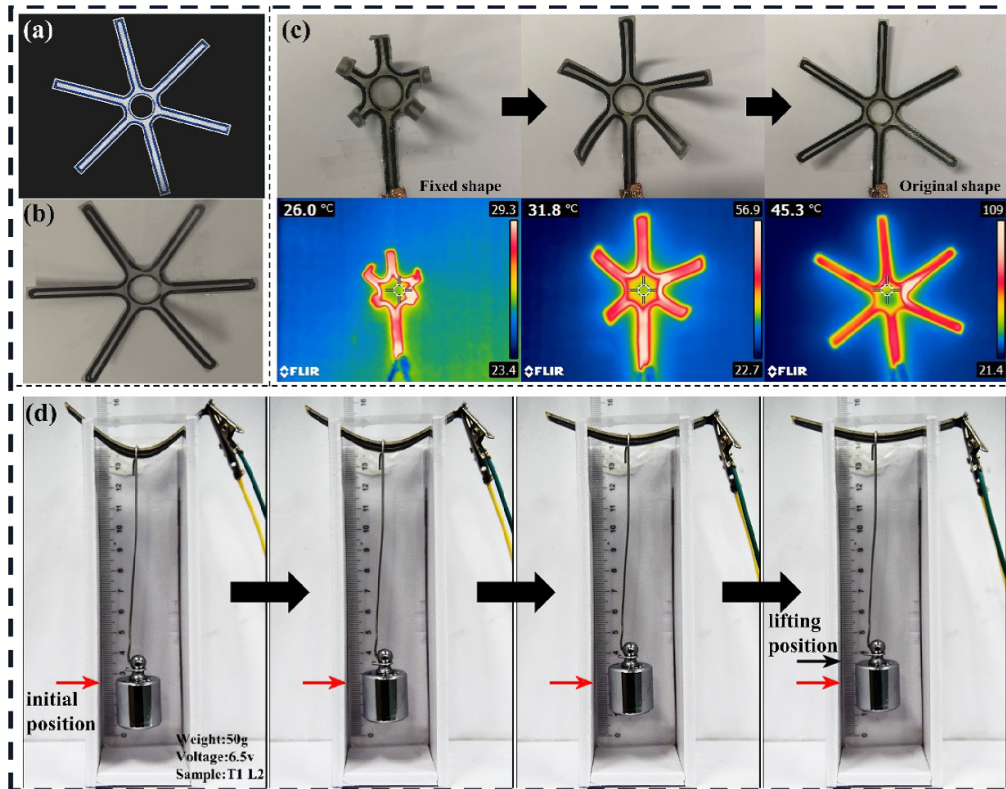


Figure 9. Applications experiment of CCF/PLA composites. (a) Model and (b) printed specimen of composite deployable claw-device. (c) The snapshots and infrared images of the claw-device during the electrothermal-actuated shape recovery process. (d) An experiment of an electrothermal actuated load-bearing lifting device.

segment of PLA melts with increasing temperature, the bent specimen attempts to straighten and generates a compressive force on the probe tip of the force sensor, which is acquired by the force value acquisition system. However, when a certain high temperature is reached, the molecular chains become softer because most part soft segment crystals were melted, and the specimen began stress relaxation.

Figure 8(a) shows the recovery force vs. temperature curves of 4D printed CCF/PLA with the same carbon fiber layer of 2L and applied voltage of 7 V at different specimen thicknesses. The maximum shape recovery force of different specimens was recorded in table 2. It can be seen that the recovery force increases with increasing the specimen thickness, and the maximum shape recovery force of T2L2V7 is about $2.38 \text{ N} \pm 0.03 \text{ N}$. Figure 8(b) shows the recovery force vs. temperature curves of specimens at different voltages. It can be found that the shape recovery force decreases with increasing the applied voltage. This is because that the shape recovery force is a slow-release process, while the high voltage generates more heat to make the molecular chain of PLA reversible phase soften quickly, thus, the recovery force starts to decline before it reaches its maximum. Figure 8(c) compares the

recovery forces of specimens with different carbon fiber layers at the same thickness and voltage. It is obvious that shape recovery force increases with increasing the carbon fiber layers, and the maximum of shape recovery force increases from $2.38 \text{ N} \pm 0.03 \text{ N}$ for a 2L specimen to about $7.38 \pm 0.03 \text{ N}$ for a 6L specimen. These shape recovery forces results are much higher than that of other articles. For example, Wang *et al* [39] tested the shape recovery force of 4D printed PLA specimens with different process parameters and the results showed that all the recovery forces were $<0.35 \text{ N}$.

3.5. Applications

Based on the electrothermal shape memory behavior of 4D printed CCF/PLA composite, one deployable claw-device was designed to demonstrate the practicality of electrothermal stimulation response behavior. Figures 9(a) and (b) show the specimen model design diagram and the printed specimen picture, respectively. The original shape specimen was predetermined to be claw-shaped, and then the fixed claw-shaped returned to nearly its original shape after approximately 2 min under a voltage of 15 V. The infrared image as shown in

figure 9(c), we can see that the temperature of the claw-shaped specimen gradually increases with increasing the time, and the specimen gradually returns to its original shape. This kind of deployable claw-device has two advantages. The first is that it can be deformed into a variety of shapes, after the device is deformed, it saves space and can be used in a variety of environments. The second is that it can be deployed after deformation and can be used to remotely drive an automatic deployment device.

We also designed a load-bearing lifting device to characterize the recovery force qualitatively as shown in figure 9(d). A bent specimen with 1 mm thickness (T1L2) lifted a 50 g weight by about 10 mm under a 6.5 V voltage, which was recorded in detail in the movie S2. Besides, we tested that the T1.5L2 and T2L2 specimens also lifted 100 g and 200 g respectively under a voltage of 6.5 V. The length and width of the load-bearing lifting device are 80 mm and 13 mm respectively. These experimental results correspond to the shape recovery force test result. This load-bearing device can be used to automatically lift structural parts. These two experiments demonstrate the potential application of 4D printed composite materials in self-actuated intelligent structures.

4. Conclusions

In summary, we have successfully designed and prepared 4D printed CCF/PLA composites and demonstrated its performance. It concluded that the introduction of continuous carbon fiber greatly enhances the mechanical properties of 4D printed CCF/PLA composite, where the storage modulus of CCF/PLA 6L is about twice that of pure PLA and the strength of CCF/PLA 6L is about 2.5 times that of pure PLA. The printed CCF/PLA composite also exhibits good electrothermal shape memory behaviors, which were primarily influenced by the specimen thickness, carbon fiber content and applied voltage. The shape recovery force increases significantly with increasing the carbon fiber layers. Finally, we demonstrated the electrothermal response behavior of a deployable claw-device and a load-bearing lifting device. The excellent electrothermal shape memory behavior, high strength, high shape recovery force, low-voltage (<16 V) response, and complex 3D printed structural design confirms the potential of functional applications of 4D printed CCF/PLA composite.

Acknowledgments

The authors acknowledge the financial supports from the Chang Jiang Scholars Program, National Science Foundation of China (Grant Numbers 51875099 and 51675095), Shanghai Sailing Program (Grant Number 19YF1401200), the Fundamental Research Funds for the Central Universities of China and the Initial Research Funds for Young Teachers of Donghua University. This work is also funded by the National Natural Science Foundation of China (Grant No. 11802075) and the China Postdoctoral Science Foundation.

ORCID iDs

Baozhong Sun  <https://orcid.org/0000-0001-9573-1145>

Bohong Gu  <https://orcid.org/0000-0003-3797-1081>

Jinsong Leng  <https://orcid.org/0000-0001-5098-9871>

Wei Zhang  <https://orcid.org/0000-0002-8809-806X>

References

- [1] Tibbitts S 2014 4D printing: multi-material shape change *Archit. Des.* **84** 116–21
- [2] Ge Q, Qi H J and Dunn M L 2013 Active materials by four-dimension printing *Appl. Phys. Lett.* **103** 1–5
- [3] Lendlein A, Jiang H, Jünger O and Langer R 2005 Light-induced shape-memory polymers *Nature* **434** 879–82
- [4] Wang W X, Liu X B, Xu W, Wei H Q, Liu Y J, Han Y, Jin P, Du H J and Leng J S 2018 Light-induced microfluidic chip based on shape memory gold nanoparticles/poly (vinyl alcohol) nanocomposites *Smart Mater. Struct.* **27** 105047
- [5] Luo H, Li Z, Yi G, Zu X, Wang H, Wang Y, Huang H, Hu J, Liang Z and Zhong B 2014 Electro-responsive silver nanowire-shape memory polymer composites *Mater. Lett.* **134** 172–5
- [6] Wei K, Zhu G M, Tang Y S, Li X M and Liu T T 2012 The effects of carbon nanotubes on electroactive shape-memory behaviors of hydro-epoxy/carbon black composite *Smart Mater. Struct.* **21** 085016
- [7] Felton S, Tolley M, Demaine E, Rus D and Wood R 2014 A method for building self-folding machines *Science* **345** 644–6
- [8] Zhang W, Zhang F, Lan X, Leng J S, Wu A S, Bryson T M, Cotton C, Gu B, Sun B and Chou T-W 2018 Shape memory behavior and recovery force of 4D printed textile functional composites *Compos. Sci. Technol.* **160** 224–30
- [9] Ge Q, Sakhaei A H, Lee H, Dunn C K, Fang N X and Dunn M L 2016 Multimaterial 4D printing with tailorable shape memory polymers *Sci. Rep.* **6** 31110
- [10] Cuevas J M, Rubio R, Laza J M, Vilas J L, Rodriguez M and Leon L M 2012 Shape memory composites based on glass-fibre-reinforced poly(ethylene)-like polymers *Smart Mater. Struct.* **21** 035004
- [11] Liu Y et al 2018 Shape memory behavior and recovery force of 4D printed laminated Miura-origami structures subjected to compressive loading *Composites B* **153** 233–42
- [12] Meng H, Mohamadian H, Stubblefield M, Jerro D, Ibekwe S, Pang S S and Li G 2013 Various shape memory effects of stimuli-responsive shape memory polymers *Smart Mater. Struct.* **22** 093001
- [13] Wang J, Wang Z, Song Z, Ren L, Liu Q and Ren L 2019 Biomimetic shape-color double-responsive 4D printing *Adv. Mater. Technol.* **4** 1900293
- [14] Hu Y et al 2020 Botanical-inspired 4D printing of hydrogel at the microscale *Adv. Funct. Mater.* **30** 1907377
- [15] Gong X-L, Xiao Y-Y, Pan M, Kang Y, Li B-J and Zhang S 2016 pH- and thermal-responsive multishape memory hydrogel *ACS Appl. Mater. Interfaces* **8** 27432–7
- [16] Cuevas J M, Alonso J, German L, Iturrondobeitia M, Laza J M, Vilas J L and Leon L M 2009 Magneto-active shape memory composites by incorporating ferromagnetic microparticles in a thermo-responsive polyalkenamer *Smart Mater. Struct.* **18** 075003
- [17] Wei H Q, Zhang Q W, Yao Y T, Liu L W, Liu Y J and Leng J S 2017 Direct-write fabrication of 4D active shape-changing structures based on a shape memory polymer and its nanocomposite *ACS Appl. Mater. Interfaces* **9** 876–83

- [18] Yu K, Liu Y and Leng J S 2014 Shape memory polymer/CNT composites and their microwave induced shape memory behaviors *RSC Adv.* **4** 2961–8
- [19] Han B *et al* 2019 Plasmonic-assisted graphene oxide artificial muscles *Adv. Mater.* **31** 1806386
- [20] Cui C, Kim D O, Pack Y M, Han B, Han L, Sun Y and Han L-H 2020 4D printing of self-folding and cell-encapsulating 3D microstructures as scaffolds for tissue-engineering applications *Biofabrication* **12** 045018
- [21] Wang W, Yu C Y, Serrano P A A and Ahn S H 2019 Soft grasping mechanisms composed of shape memory polymer based self-bending units *Composites B* **164** 198–204
- [22] Truby R L, Wehner M, Grosskopf A K, Vogt D M, Uzel S G M, Wood R J and Lewis J A 2018 Soft somatosensitive actuators via embedded 3D printing *Adv. Mater.* **30** 1706383
- [23] Hu W, Lum G Z, Mastrangeli M and Sitti M 2018 Small-scale soft-bodied robot with multimodal locomotion *Nature* **554** 81–85
- [24] Xia L, Gao H, Bi W, Fu W, Qiu G and Xin Z 2019 Shape memory behavior of carbon black-reinforced trans-1,4-polyisoprene and low-density polyethylene composites *Polymers* **11** 807
- [25] Xu Z, Ding C, Wei D-W, Bao R-Y, Ke K, Liu Z, Yang M-B and Yang W 2019 Electro and light active actuators based on reversible shape-memory polymer composites with segregated conductive networks *ACS Appl. Mater. Interfaces* **11** 30332–40
- [26] Liu Y, Zhang F, Leng J S, Fu K, Lu X L, Wang L, Cotton C, Sun B, Gu B and Chou T-W 2019 Remotely and sequentially controlled actuation of electroactivated carbon nanotube/shape memory polymer composites *Adv. Mater. Technol.* **4** 1900600
- [27] Garces I T and Ayranci C 2020 Active control of 4D prints: towards 4D printed reliable actuators and sensors *Sensors Actuators A* **301** 111717
- [28] Sun Y, Chen H J, Yin H, Sun B Z, Gu B H and Zhang W 2020 A flexible, high-strength, conductive shape memory composite fabric based on continuous carbon fiber/polyurethane yarn *Smart Mater. Struct.* **29** 085044
- [29] Luo X and Mather P T 2010 Conductive shape memory nanocomposites for high speed electrical actuation *Soft Matter* **6** 2146–9
- [30] Wei H, Cauchy X, Navas I O, Abderrafai Y, Chizari K, Sundararaj U, Liu Y, Leng J S and Theriault D 2019 Direct 3D printing of hybrid nanofiber-based nanocomposites for highly conductive and shape memory applications *ACS Appl. Mater. Interfaces* **11** 24523–32
- [31] Zeng C, Liu L, Bian W, Liu Y and Leng J S 2020 4D printed electro-induced continuous carbon fiber reinforced shape memory polymer composites with excellent bending resistance *Composites B* **194** 108034
- [32] Zhang F, Xia Y, Wang L, Liu L, Liu Y and Leng J S 2018 Conductive shape memory microfiber membranes with core-shell structures and electroactive performance *ACS Appl. Mater. Interfaces* **10** 35526–32
- [33] Gall K, Dunn M L, Liu Y, Finch D, Lake M and Munshi N A 2002 Shape memory polymer nanocomposites *Acta Mater.* **50** 5115–26
- [34] Chen L, Li W, Liu Y and Leng J S 2015 Epoxy shape-memory polymer reinforced by thermally reduced graphite oxide: influence of processing techniques *J. Appl. Polym. Sci.* **132** 42502
- [35] Liu Y, Zhang W, Zhang F, Leng J S, Pei S, Wang L, Jia X, Cotton C, Sun B and Chou T-W 2019 Microstructural design for enhanced shape memory behavior of 4D printed composites based on carbon nanotube/poly(lactic acid) filament *Compos. Sci. Technol.* **181** 107692
- [36] Monzón M D, Paz R, Pei E, Ortega F, Suárez A, Ortega Z, Alemán M E, Plucinski T and Clow N 2017 4D printing: processability and measurement of recovery force in shape memory polymers *Int. J. Adv. Manuf. Technol.* **89** 1827–36
- [37] Song J J, Chang H H and Naguib H E 2015 Biocompatible shape memory polymer actuators with high force capabilities *Eur. Polym. J.* **67** 186–98
- [38] ASTM D7264/D7264M-15 2015 *Standard Test Method for Flexural Properties of Polymer Matrix Composite Materials* (West Conshohocken, PA: ASTM International)
- [39] Wang J, Wang Z, Song Z, Ren L, Liu Q and Ren L 2019 Programming multistage shape memory and variable recovery force with 4D printing parameters *Adv. Mater. Technol.* **4** 1900535